IEEE Photonics Journal
An IEEE Photonics Society Publication

Switchable and Tunable Microwave Photonic Brillouin-Based Filter

Volume 4, Number 5, October 2012

Weiwei Zhang
Robert A. Minasian, Fellow, IEEE

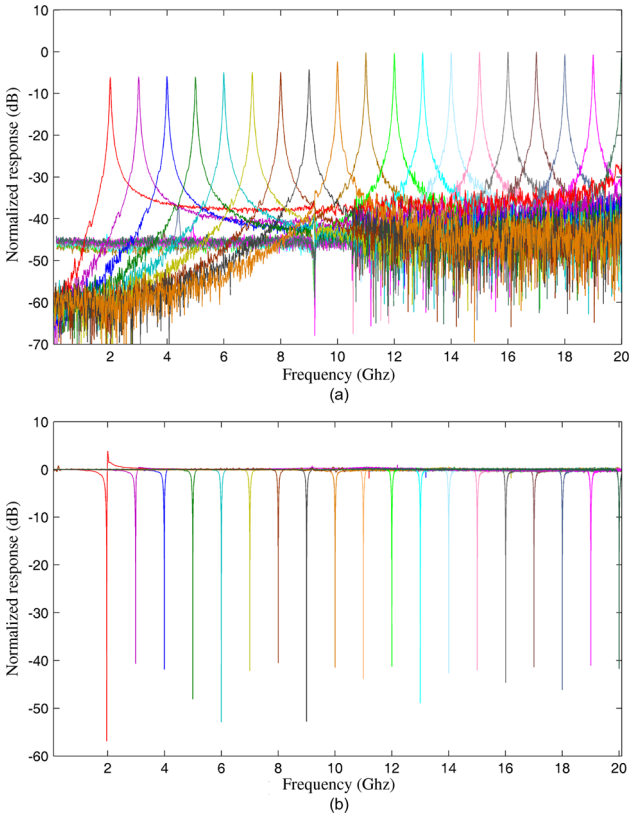

DOI: 10.1109/JPHOT.2012.2209114
1943-0655/$31.00 ©2012 IEEE

Switchable and Tunable Microwave Photonic Brillouin-Based Filter

Weiwei Zhang and Robert A. Minasian, *Fellow, IEEE*

School of Electrical and Information Engineering, Institute of Photonics and Optical Science, University of Sydney, Sydney, N.S.W. 2006, Australia

DOI: 10.1109/JPHOT.2012.2209114
1943-0655/$31.00 ©2012 IEEE

Manuscript received June 13, 2012; revised July 8, 2012; accepted July 10, 2012. Date of publication July 17, 2012; date of current version August 6, 2012. This work was supported by the Australian Research Council. Corresponding author: W. Zhang (e-mail: weiwei.zhang@sydney.edu.au).

Abstract: A new structure that realizes a switchable microwave photonic filter, which can be readily switched between a bandpass filter and a notch filter, is presented. It is based on optical processing the sidebands of the RF-modulated signal that is obtained after a dual-drive Mach–Zehnder modulator (DDMZM), using stimulated Brillouin scattering (SBS) effects. Switching of the filter function is simply and conveniently obtained by changing the dc bias to the DDMZM. In addition, the center frequency of the switchable filter can be tuned over a wide frequency range. A detailed analysis and simulation of the DDMZM operation in conjunction with the SBS technique is presented in order to obtain the required optimum bias conditions for the DDMZM for realizing the switching action between the single-bandpass filter and the notch filter and also to select the optimum pump power for the SBS operation. Experimental results demonstrate the ability of this structure to switch between a high-resolution bandpass filter and a high-resolution notch filter, with Q values around 400–500, and the ability to operate over a frequency range of 2–20 GHz.

Index Terms: Microwave photonic filter, stimulated Brillouin scatter, microwave photonics, signal processing.

1. Introduction

Photonic signal processing, using photonic approaches to condition microwave and radio-frequency (RF) signals, is attractive due to the inherent advantages of high time–bandwidth product and immunity to electromagnetic interference (EMI) [1]–[3].

A range of photonic signal processor structures has been reported to realize either a bandpass filter or a notch filter [4]–[16], including methods to generate multiple optical carriers and manipulate their amplitudes to increase and control the number of taps [14]–[16]. However, these do not meet the requirements of multifunction applications that require the ability to switch the filtering function between a bandpass filter and a notch filter to provide the needed capability where both channel selection and channel rejection are needed. There have been very few reports on switchable microwave photonic filters. In [17], switchable filtering was proposed by switching the optical transmission of optical modulators between their maximum and minimum values; however, this approach requires many modulators to realize high-resolution filtering performance, and it also has phase-induced intensity noise limitations. In [18], switching of filtering was proposed by rotating the half-wave plate of a variable polarization beamsplitter of a Sagnac interferometer loop; however, the performance was limited by the two-tap finite-impulse response structure, which does not enable the realization of high-resolution filtering. In [19], a switchable microwave photonic filter between the bandpass and notch filter response was proposed by tuning two optical tunable bandpass filters

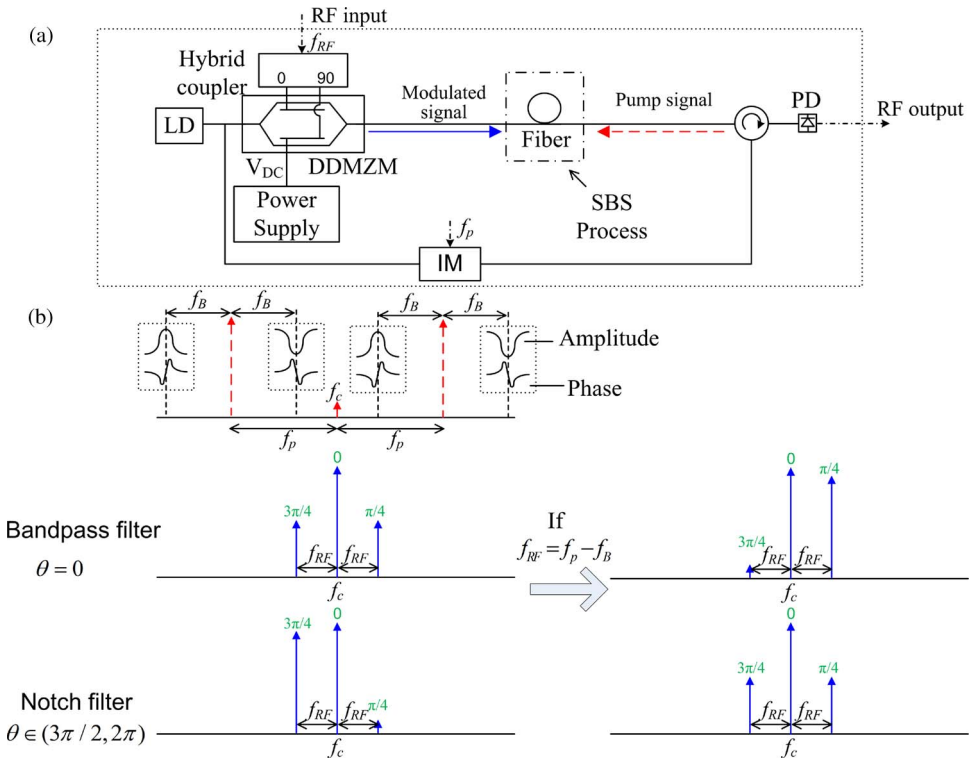

Fig. 1. Operational principle of the switchable filter (a) structure; (b) spectra.

connected to an amplified recirculating delay line loop; however, this is limited by the very small free spectrum range and periodic response that results from the loop length and also by the large phase-induced intensity noise generated.

In this paper, we report a new structure that enables the realization of a switchable microwave photonic filter that can be switched between a bandpass filter and a stopband notch filter response, using simple and rapid control. It is based on a stimulated Brillouin scattering (SBS) technique in conjunction with a dual-drive Mach–Zehnder modulator (DDMZM) that processes the sidebands of the RF-modulated signal. Switching of the filter function is simply and conveniently obtained by changing the dc bias to the DDMZM. In addition, the center frequency of the switchable filter can be tuned over a wide frequency range. We present a detailed analysis and simulation of the DDMZM operation in conjunction with the SBS technique in order to determine the optimum bias conditions that are required to be chosen for the DDMZM in order to realize the switching action and also to select the optimum pump power for the SBS operation. Experimental results are presented, which demonstrate the ability of this structure to switch between a high-resolution bandpass filter and a high-resolution notch filter, with Q values around 400–500, and the ability to operate over a wide frequency range of 2–20 GHz.

2. Principle of Operation and Theory

The structure of the new switchable microwave photonic filter is shown in Fig. 1(a). Light from a laser is passed into the DDMZM in the upper arm, which is driven by the RF signal f_{RF} that is fed through a quadrature hybrid coupler. The DDMZM also has a control voltage bias V_{dc}. The modulated signal is launched into a length of fiber where SBS occurs in the presence of the counter-propagating pump. The pump light is obtained from the same laser at optical frequency f_c; hence, stable SBS operation is realized [20]. The pump light is modulated at RF frequency f_p by a low-biased intensity modulator, which generates a double-sideband suppressed-carrier signal and is

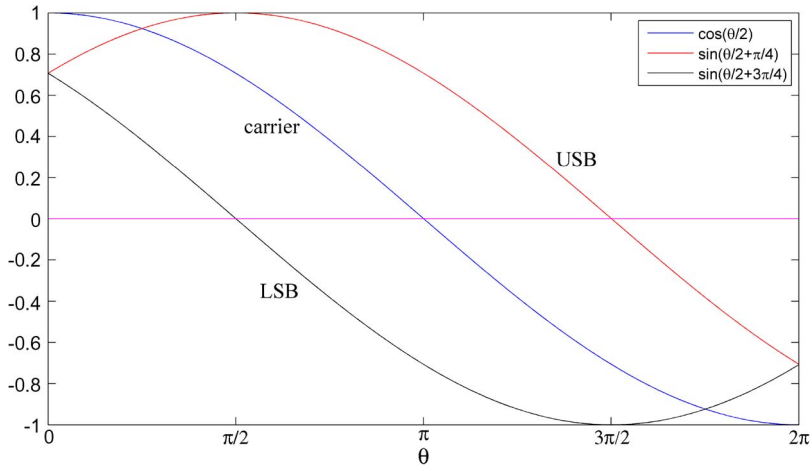

Fig. 2. Coefficients of the carrier, lower sideband (LSB), and upper sideband (USB).

used to tune the filter frequency by changing the positions of the SBS gain and loss. The filter switching function is achieved by changing the dc bias voltage V_{dc} of the DDMZM.

For the DDMZM, which comprises a Mach–Zehnder structure with two phase modulators in each arm and a dc bias in one arm and which is driven via a 3-dB quadrature hybrid coupler to generate two RF signals with the same amplitude and $\pi/2$ phase difference, the induced phase for both arms is given by

$$\Psi_1 = \theta + m\sin(2\pi f_{RF}t) \tag{1}$$

$$\Psi_2 = m\cos(2\pi f_{RF}t) \tag{2}$$

where $\theta = \pi V_{dc}/V_\pi$ is the phase induced by the dc bias voltage, $m = \pi V_{RF}/(\sqrt{2}V_\pi)$ is the phase induced by the RF signal, f_{RF} represents the frequency of the input RF signal, and V_π denotes the half-wave voltage of the modulator.

The switching function relies on controlling of the state of the DDMZM. Under small-signal modulation, and by considering only the first-order sidebands, the output optical field after the DDMZM is given by

$$E = \frac{E_0}{2}\left[(e^{j\theta}+1)J_0(m)e^{j2\pi f_c t} + (e^{j\theta}+j)J_1(m)e^{j2\pi(f_c+f_{RF})t} - (e^{j\theta}-j)J_1(m)e^{j2\pi(f_c-f_{RF})t}\right] \tag{3}$$

where E_0 represents the amplitude of the input laser, and $J_n(\cdot)$ denotes the nth-order Bessel function of the first kind with $n = 0, \pm 1$. The first term in (3) corresponds to the carrier, and the second and third terms correspond to the upper (USB) and lower (LSB) sidebands. From (3), it is clear that the amplitudes and phases of the carrier and the two sidebands are determined by the dc-induced phase θ. In order to elucidate the dc-induced phase effect in more detail, (3) is represented by

$$E = E_0 e^{j2\pi f_c t + j\frac{\theta}{2}}\left[\cos\frac{\theta}{2}J_0(m) + \sin\left(\frac{\theta}{2}+\frac{\pi}{4}\right)J_1(m)e^{j2\pi f_{RF}t + j\frac{\pi}{4}} + \sin\left(\frac{\theta}{2}+\frac{3\pi}{4}\right)J_1(m)e^{-j2\pi f_{RF}t + j\frac{3\pi}{4}}\right]. \tag{4}$$

This shows that the relative phase differences between the carrier and the sidebands are determined by the signs of the coefficients for each of the three terms in (4). The coefficients as the function of the dc voltage-induced phase for the carrier and two sidebands are shown in Fig. 2.

When $\theta \in (0, \pi/2)$, it can be seen that all the three coefficients are positive. Thus, the phase difference between the upper sideband and the carrier is $\pi/4$, while the phase difference between the

carrier and the lower sideband is $-3\pi/4$. In this situation, the beating signals between the carrier and the two sidebands are out-of-phase. Similarly, if $\theta \in (\pi/2, \pi)$, it can be seen that the coefficient of the third term in (4) is negative, while the other two coefficients are positive. As a result, the phase difference between the upper sideband and the carrier stays the same at $\pi/4$, while the phase difference between the carrier and the lower sideband changes to $\pi/4$. The beating signals between the carrier and the two sidebands now become in-phase. In the same way, it can be seen that the beating signals are in-phase if $\theta \in (\pi, 3\pi/2)$, and the beating signals are out-of-phase if $\theta \in (3\pi/2, 2\pi)$. A case of particular interest occurs when θ equals to 0 or 2π, because under these bias conditions, the amplitudes of the upper sideband and the lower sideband are the same, while the beating signals between the carrier and the two sidebands are out-of-phase. In this situation, the DDMZM acts as a phase modulator, but with the two sidebands of the output modulated signal having a factor of $\sqrt{2}/2$ compared with the traditional phase modulator, as shown in Fig. 2. Moreover, if θ equals to π, the DDMZM functions as a double-sideband suppressed-carrier modulator, since the coefficient of the first term in (4) equals to zero. Similarly, if θ equals to $\pi/2$ or $3\pi/2$, the DDMZM functions as a single-sideband modulator, with the lower sideband or upper sideband suppressed, respectively.

In order to realize the switchable microwave photonic filter, we select $\theta = 0$ to implement the bandpass filter, and we select $\theta \in (3\pi/2, 2\pi)$ to implement the notch filter. Note that switching between these two filter functions is simply obtained by changing the bias voltage to the DDMZM, which can be easily done.

The SBS process occurs in the fiber between the RF-modulated signal and the pump signal. The intensity modulator IM in the lower branch of Fig. 1(a) is biased at the minimum transmission point to generate a double-sideband suppressed-carrier signal as the SBS pump. Each sideband of the pump signal introduces both SBS gain and SBS loss spectra at frequency f_B away from the sideband, where f_B is the Brillouin frequency shift. Considering the case where $f_p > f_B$, the SBS gain and loss spectra are shown in the upper part of Fig. 1(b). Considering the SBS effect close to the carrier, SBS gain and SBS loss can be described as [21]

$$g(f_c + f) = \frac{g_0 I_p}{2} \frac{(\gamma_B/2)^2}{(-f_p + f_B + f)^2 + (\gamma_B/2)^2} + j\frac{g_0 I_p}{4} \frac{\gamma_B(-f_p + f_B + f)}{(-f_p + f_B + f)^2 + (\gamma_B/2)^2} \tag{5}$$

$$\alpha(f_c - f) = -\frac{g_0 I_p}{2} \frac{(\gamma_B/2)^2}{(-f_p + f_B + f)^2 + (\gamma_B/2)^2} + j\frac{g_0 I_p}{4} \frac{\gamma_B(-f_p + f_B + f)}{(-f_p + f_B + f)^2 + (\gamma_B/2)^2} \tag{6}$$

where g_0 and γ_B represent the line-center gain factor and Brillouin linewidth of the fiber, I_P is the intensity of each sideband of the pump wave, and f denotes the frequency offset to the carrier.

Following the SBS operation, the optical field of the forward-propagating RF-modulated signal is given by

$$E = \frac{E_0 e^{j2\pi f_c t}}{2}\left[(e^{j\theta} + 1)J_0(m) + (e^{j\theta} + j)J_1(m)e^{g(f_c + f_{RF})L + j2\pi f_{RF} t} - (e^{j\theta} - j)J_1(m)e^{\alpha(f_c - f_{RF})L - j2\pi f_{RF} t}\right] \tag{7}$$

where L is the length of the fiber. Omitting the dc and the small second harmonic components, the optical power incident on the photodetector (PD) is given by

$$\begin{aligned} P \approx \frac{\sqrt{2}}{2} P_0 \alpha_0 J_0(m) J_1(m) \Big\{ & \Big[(1 + \sin\theta + \cos\theta) G(f_{RF}) \cos\left(\phi(f_{RF}) + \frac{\pi}{4}\right) \\ & - (1 - \sin\theta + \cos\theta) A(f_{RF}) \cos\left(\phi(f_{RF}) - \frac{\pi}{4}\right)\Big] \cdot \cos(2\pi f_{RF} t) \\ & - \Big[(1 + \sin\theta + \cos\theta) G(f_{RF}) \sin\left(\phi(f_{RF}) + \frac{\pi}{4}\right) \\ & + (1 - \sin\theta + \cos\theta) A(f_{RF}) \sin\left(\phi(f_{RF}) - \frac{\pi}{4}\right)\Big] \cdot \sin(2\pi f_{RF} t) \Big\} \end{aligned} \tag{8}$$

where P_0 is the optical power of the light before DDMZM, α_0 is the optical loss between the laser output and the PD input, and

$$G(f_{\mathrm{RF}}) = e^{\mathrm{Re}(g(f_c+f_{\mathrm{RF}}))L} = e^{\frac{g_0 I_p L}{2}\frac{(\gamma_B/2)^2}{(-f_p+f_B+f_{\mathrm{RF}})^2+(\gamma_B/2)^2}} \tag{9}$$

$$A(f_{\mathrm{RF}}) = e^{\mathrm{Re}(\alpha(f_c-f_{\mathrm{RF}}))L} = e^{-\frac{g_0 I_p L}{2}\frac{(\gamma_B/2)^2}{(-f_p+f_B+f_{\mathrm{RF}})^2+(\gamma_B/2)^2}} \tag{10}$$

$$\phi(f_{\mathrm{RF}}) = \mathrm{Im}(\alpha(f_c - f_{\mathrm{RF}}))L = \mathrm{Im}(g(f_c + f_{\mathrm{RF}}))L = \frac{g_0 I_p L}{4}\frac{\gamma_B(-f_p + f_B + f_{\mathrm{RF}})}{(-f_p + f_B + f_{\mathrm{RF}})^2 + (\gamma_B/2)^2}. \tag{11}$$

Thus, the RF power at the PD is given by

$$\begin{aligned} P_{\mathrm{RF\ out}} = \langle P^2\Re^2\rangle Z_o = \frac{1}{4}\Re^2 Z_0 P_0^2\alpha_0^2 J_0^2(m)J_1^2(m) \\ \times\Big[(1+\sin\theta+\cos\theta)^2 G^2(f_{\mathrm{RF}}) + (1-\sin\theta+\cos\theta)^2 A^2(f_{\mathrm{RF}}) \\ - 2A(f_{\mathrm{RF}})G(f_{\mathrm{RF}})(1+\sin\theta+\cos\theta)(1-\sin\theta+\cos\theta)\cos(2\phi(f_{\mathrm{RF}}))\Big] \end{aligned} \tag{12}$$

where $\Re$ represents the PD responsivity, and Z_o is the load resistance. Through (12), the SBS gain, loss, and SBS-induced nonlinear phase are mapped from the optical domain to the RF domain. The mapping function is mainly determined by the dc-induced phase bias of the DDMZM. By changing the phase bias, different frequency responses can be implemented.

In order to realize bandpass filtering, it is required that the amplitudes for the two sidebands are equal and that the beating signals between the carrier and the two sidebands are out-of-phase, prior to the application of the SBS effect, as illustrated in Fig. 1(b). Thus, $\theta = 0$ must be selected so that the DDMZM operates as a phase modulator, as discussed above. The optical spectrum of the modulated signal is schematically illustrated in Fig. 1(b) labeled bandpass filter. At the output of the DDMZM, the two sidebands are out-of-phase and have equal amplitude. Only the RF signal with the frequency of $f_{\mathrm{RF}} = f_p - f_B$ undergoes the SBS effect, which consequently breaks the amplitude equality between the sidebands since the lower sideband of the RF-modulated signal is significantly attenuated while the upper sideband is amplified, as shown on the right-hand side of Fig. 1(b). This creates a bandpass response, and an RF signal is generated at the PD output because the beating between the carrier and the upper sideband is significantly larger than the beating between the carrier and the lower sideband. The RF power at the output of the PD is given by [11]

$$P_{\mathrm{RF\ out}} = \Re^2 Z_o P_0^2\alpha_0^2 J_0^2(m)J_1^2(m)\big[A^2(f_{\mathrm{RF}}) + G^2(f_{\mathrm{RF}}) - 2A(f_{\mathrm{RF}})G(f_{\mathrm{RF}})\cos(2\phi(f_{\mathrm{RF}}))\big]. \tag{13}$$

For other RF frequencies, there is no RF signal at the PD output because the SBS has no effect on the phase-modulated signal (the RF signal after DDMZM with $\theta = 0$). Hence, a single-bandpass microwave photonic filter with central frequency of $f_p - f_B$ is realized.

We next select θ to be in the range $\theta \in (3\pi/2, 2\pi)$, so that the phase difference between the upper sideband and the carrier is $\pi/4$, while the phase difference between the lower sideband and the carrier is $3\pi/4$. The optical spectrum of the modulated signal is schematically illustrated in Fig. 1(b) labeled notch filter. As can be seen, the beatings of the carrier and the two sidebands are out-of-phase, and in addition, at the output of the DDMZM, the amplitude of the lower sideband is larger than the amplitude of the upper sideband. Hence, an RF signal is obtained at the PD output at all frequencies, where the SBS-induced gain and loss is far away from the two sidebands. However, when the input RF frequency is $f_{\mathrm{RF}} = f_p - f_B$, and the amplitudes of the two sidebands are equalized by properly choosing the SBS pump power and the phase bias θ, as shown on the right-hand side of Fig. 1(b), the beatings between the carrier and the two sidebands are out-of-phase and fully cancel. Thus, there is no RF signal at the PD output, and a notch response is realized at the frequency of $f_p - f_B$.

TABLE 1
Parameters for simulation

Parameter	Value	Unit
$\Re$	0.65	A/W
Z_i	50	ohm
Z_o	50	ohm
P_0	10	dBm
α_0	0.1	
V_π	5.3	V
γ_B	40	MHz
f_B	9.21	GHz
f_p	19.21	GHz

In summary, a switchable microwave photonic filter at the center frequency of $f_p - f_B$ is realized, in which the switching function is easily accomplished by changing the dc bias of the DDMZM. The frequency where the switched filtering occurs can also be tuned by changing the drive frequency f_p.

For completeness, it can be noted that though the SBS gain at frequency $f_c - f_p - f_B$ and the SBS loss at frequency $f_c + f_p + f_B$ are not included in (5) and (6), these introduce an additional bandpass response at frequency $f_p + f_B$; however, since $f_p + f_B$ is very high, it can be eliminated by ensuring it falls outside the bandwidth of the PD.

3. Simulation Results

Simulations were conducted to investigate the frequency response and the design of the proposed structure, in order to choose the optimum dc voltage-induced phase bias of the DDMZM and the SBS gain/loss. Using (12), the transfer function of the structure can be written as

$$|H(f)|^2 = \frac{P_{\text{RF out}}}{P_{\text{RF in}}} \approx \frac{\pi^2 \Re^2 Z_i Z_o P_0^2 \alpha_0^2}{16 V_\pi^2} \times \Big[(1 + \sin\theta + \cos\theta)^2 G^2(f_{\text{RF}}) + (1 - \sin\theta + \cos\theta)^2 A^2(f_{\text{RF}}) - 2A(f_{\text{RF}})G(f_{\text{RF}})(1 + \sin\theta + \cos\theta)(1 - \sin\theta + \cos\theta)\cos(2\phi(f_{\text{RF}}))\Big] \quad (14)$$

where $J_0(m) \approx 1$ and $J_1(m) \approx m/2$ for small-signal approximation. Here, Z_i is the input impedance of the DDMZM. The parameters for the simulation are listed in Table 1.

Fig. 3 shows the calculated frequency response for any specified dc voltage-induced phase bias θ and for SBS gain values of 25 and 5 dB. It can be seen that, in general, a range of response types can be obtained as θ is varied over its full range from 0 to 2π, including a bandpass response, a dual notch with an intervening bandpass response, and a notch response. Here, we focus on the filter responses of interest for switching, namely, the bandpass response and the notch response. For high SBS pump, the proposed structure can work as a single-passband filter or a single-notch filter, as shown in Fig. 3(a). A single-passband filter can be realized within a relatively wide range of the phase bias conditions; however, the phase bias range for a single-notch filter is very small. On the other hand, for low SBS pump, a single-notch filter can be realized over a range of phase bias conditions; however, the phase bias for a single-passband filter with good performance becomes restricted to only the phase bias value of 0, as shown in Fig. 3(b).

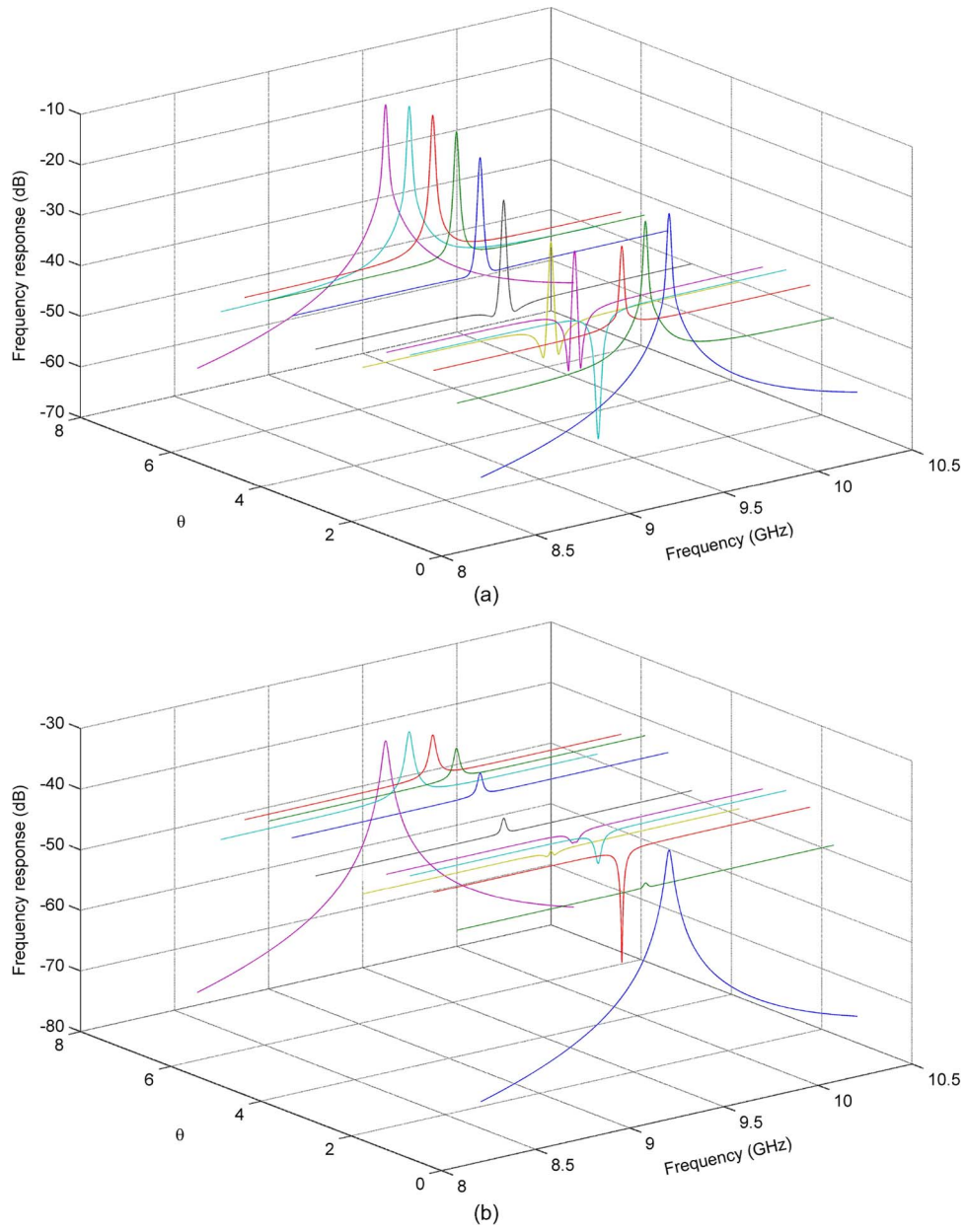

Fig. 3. Calculated frequency response of phase bias θ when the central SBS gain $|G(f_B)|^2$ is (a) 25 dB; (b) 5 dB.

If θ is chosen to be close to 0 or 2π, the proposed structure functions as a single-bandpass filter. The out-of-band rejection ratio for the bandpass filter can be derived from (14) as

$$\text{OOBR} = 10\log\frac{\left((1-\sin\theta+\cos\theta)A(f_p-f_B)-(1+\sin\theta+\cos\theta)G(f_p-f_B)\right)^2}{4\sin^2\theta}\ \text{dB}. \qquad (15)$$

Fig. 4 shows the effect of the dc voltage-induced phase bias θ on the out-of-band rejection ratio of the bandpass filter for three different SBS gain values of 25, 15, and 5 dB. It can be seen that the maximum out-of-band rejection ratio of the bandpass filter is realized for any SBS gain when $\theta = 0$, which corresponds to phase modulation for the DDMZM. In this case, the obtained out-of-band

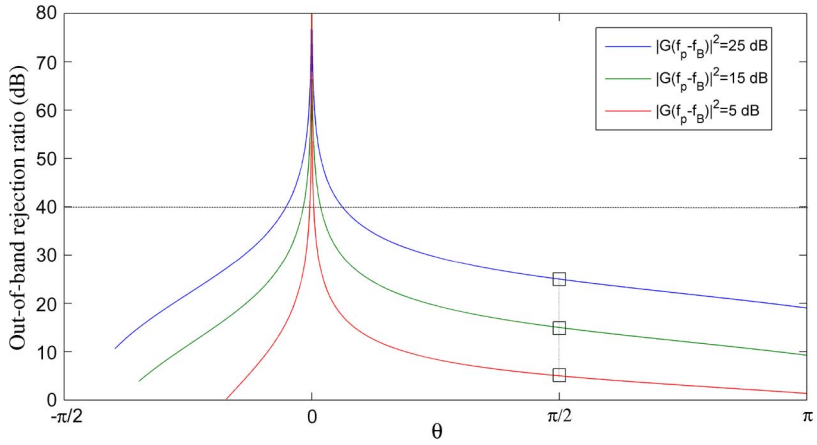

Fig. 4. Calculated out-of-band rejection ratios of the bandpass filter as a function of the dc voltage-induced phase bias θ for SBS gain values of 25, 15, and 5 dB.

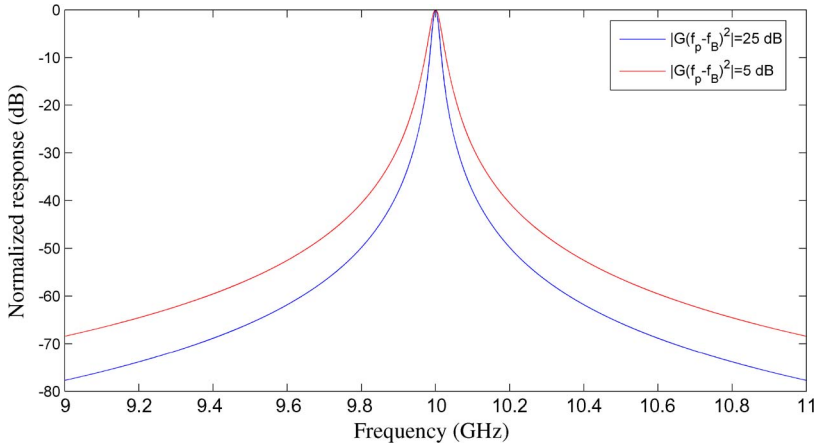

Fig. 5. Calculated optimized bandpass responses for SBS gain values of 25 and 5 dB.

rejection ratio performance is improved compared with that realized by previous single-sideband modulator approaches [10], [12], which correspond to $\theta = \pi/2$, as is shown in Fig. 4, especially when the pump power is low. Fig. 4 also shows that the tolerance of θ around its optimum value of 0 is good, for obtaining a high out-of-band rejection ratio of $>$ 40 dB, and that the tolerance improves as the SBS gain increases. Fig. 5 shows the normalized response for a bandpass filter designed to operate with a center frequency of 10 GHz, when the dc voltage-induced phase bias is $\theta = 0$, for both high SBS gain and low SBS gain. This shows that for the bandpass filter, a high SBS gain, which corresponds to high pump power, produces a narrower response. Hence, high SBS gain is desirable for realizing the bandpass filter.

We now consider the notch filter operation of the proposed structure. The notch depth of the notch filter can be derived from (14) and is given by

$$\mathrm{ND} = 10\log\frac{4\sin^2\theta}{\left((1-\sin\theta+\cos\theta)A(f_p-f_B)-(1+\sin\theta+\cos\theta)G(f_p-f_B)\right)^2}\ \mathrm{dB}. \tag{16}$$

Fig. 6 shows the effect of the dc voltage-induced phase bias θ on the notch depth of the notch filter for three different SBS gain values of 25, 15, and 5 dB. It can be seen that the optimum value of

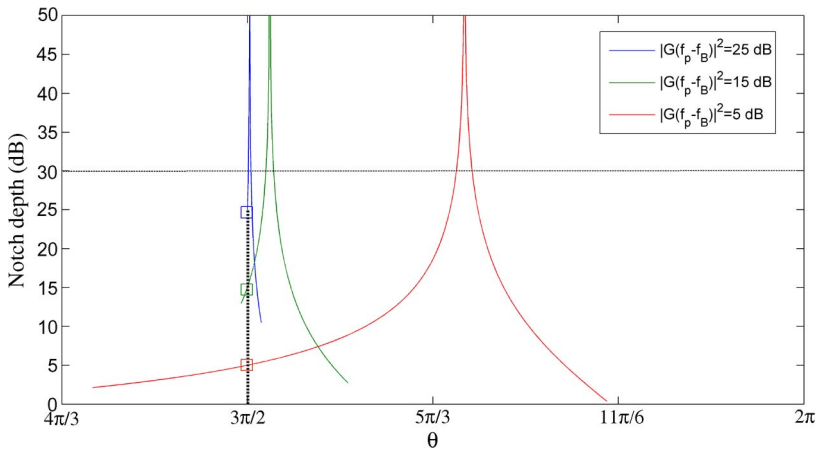

Fig. 6. Calculated notch depths of the notch filter as a function of the dc voltage-induced phase bias θ for SBS gain values of 25, 15, and 5 dB.

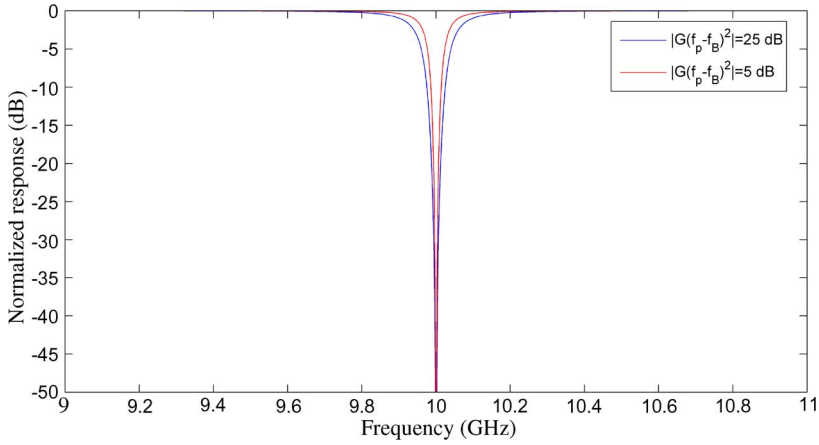

Fig. 7. Calculated optimized notch responses for SBS gain values of 25 and 5 dB.

θ for the notch filter is no longer constant, but it depends on the value of the SBS gain. The optimum phase bias θ for realizing maximum notch depth is given by

$$\theta_{\text{notch}} = 2\pi - 2\tan^{-1}\frac{G(f_p - f_B) - A(f_p - f_B)}{G(f_p - f_B) + A(f_p - f_B)} \tag{17}$$

which can be derived from (16) by letting denominator equal to 0. For small pump power, the value of θ_{notch} lies between $3\pi/2$ and 2π and approaches $3\pi/2$ as the SBS gain increases.

However, Fig. 6 also shows that phase condition required for obtaining a notch response is much stricter than that for the bandpass response, and particularly, if the SBS gain is increased, then the tolerance to the value of θ becomes very strict. Hence, operation with θ very close to $3\pi/2$, which corresponds to the DDMZM operating as a single-sideband modulator with the upper sideband suppressed, is not desirable.

Fig. 7 shows the normalized response for a notch filter designed to operate with a center frequency of 10 GHz, when the optimum dc voltage-induced phase bias is chosen, i.e., $\theta = 1.502\pi$ for an SBS gain of 25 dB and $\theta = 1.695\pi$ for an SBS gain of 5 dB. This shows that for the notch filter, a low SBS gain, which corresponds to low pump power, produces a narrower response.

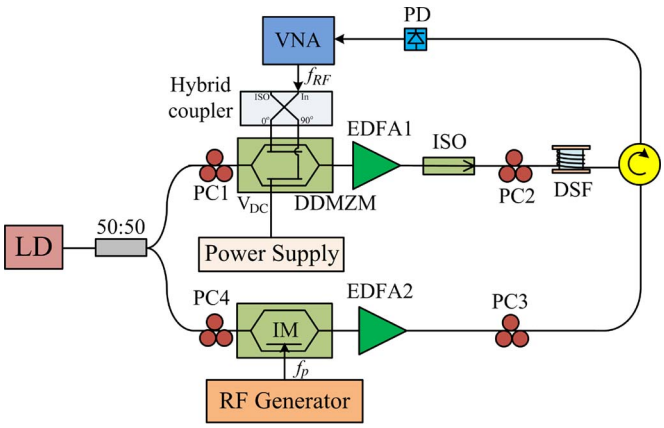

Fig. 8. Experimental setup of the switchable microwave photonic filter.

Hence, low SBS gain is desirable for realizing the notch filter, from the point of view of notch width and tolerance to operating phase bias range; however, reducing the gain also decreases power level for the passband.

Since a high SBS gain is desirable for bandpass filter realization whereas a lower SBS gain is desirable for notch filter realization, a tradeoff is required, and as a compromise, moderate SBS gain and pump power is chosen to optimize the proposed switchable photonic filter.

4. Experimental Setup and Measurements

Experiments were setup to demonstrate the proof of principle. The experimental setup of the switchable microwave photonic filter is shown in Fig. 8. Light from a laser diode (LD), operating at 1550 nm and with an output of 10 dBm, was split using a 3-dB coupler and fed into the two branches. The upper branch comprised a DDMZM driven by the RF input signal f_{RF} obtained from the vector network analyzer (VNA) after passing through a 4–44-GHz 3-dB quadrature hybrid coupler. The bandwidth of the DDMZM was 40 GHz. The dc bias of the DDMZM could be controlled between 0 and 11 V using a power supply that had a precision of 1 mV. The DDMZM had a maximum transmission point at a measured bias of 0.525 V, and the half-wave voltage of the DDMZM was measured as 5.215 V. Polarization controller1 (PC1) was used to align the polarization state of the input light into the DDMZM, and after amplification by an erbium-doped fiber amplifier1 (EDFA1), the RF-modulated signal was launched into a 1-km length of high nonlinear dispersion-shifted fiber (DSF). The DSF had a high Brillouin gain coefficient because of its small core size. Light from the laser coupled into the lower branch was fed into an IM after PC4, which was used to align the polarization state. The bandwidth of the IM was 20 GHz. The IM was biased at its minimum transmission point and was driven by an RF generator to generate a double-sideband suppressed-carrier modulation signal as the SBS pump. Tunability was realized by changing the RF frequency drive to the IM. The double-sideband suppressed-carrier signal was amplified by EDFA2. This SBS pump signal was launched by means of the optical circulator in the counter-propagating direction into the DSF. The isolator (ISO) in the upper branch was used to eliminate the pump wave after it passed through the DSF.

The SBS process occurred in the DSF between the RF-modulated signal and the pump signal. The Brillouin frequency shift of the DSF was 9.21 GHz. The SBS effect was optimized using PC2 and PC3 by adjusting the polarizations of the two counter-propagating signals [22]. After the DSF, the optical signal was detected by a PD. The frequency response of the structure was measured using the VNA with a maximum sweeping frequency of 20 GHz.

First, the switching function of the proposed structure was demonstrated for a filter frequency of 17 GHz. To obtain this, the driving RF frequency to the IM was set to 26.21 GHz. A bandpass response was realized by setting the dc bias of the DDMZM to 0.525 V, which corresponds to the

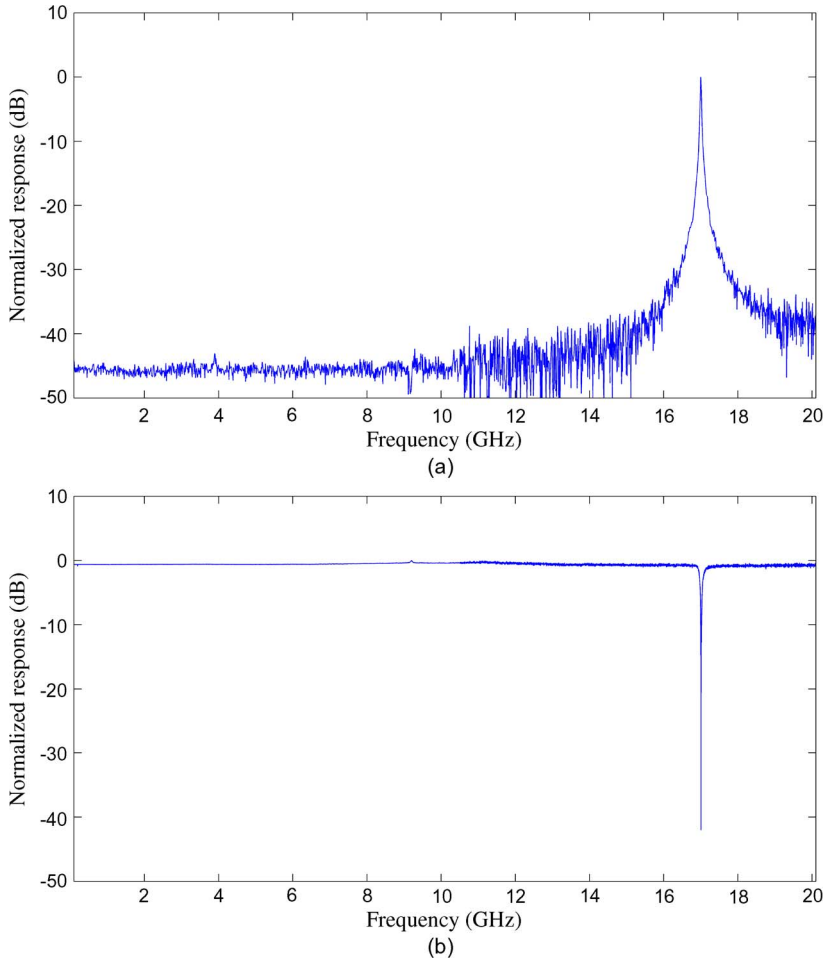

Fig. 9. Measured switching function of the filter form: (a) bandpass response; (b) notch response.

DDMZM operating as a phase modulator. Fig. 9(a) shows the measured normalized frequency response of the bandpass microwave photonic filter. The pump power of the double-sideband suppressed-carrier modulation signal was 6.2 dBm, and the optical power of the output signal injected to the PD was around 0 dBm. The bandpass center frequency is 17 GHz, which equals the frequency difference between the IM driving RF frequency and Brillouin frequency shift. The -3-dB bandwidth is about 31 MHz. This corresponds to a Q value of 594. Note that there is a single-passband response over the full 0–20-GHz measurement range. The out-of-band rejection ratio is greater than 35 dB. Next, in order to switch the function to a notch filter, the bias voltage to the DDMZM was changed to 8.591 V, which corresponds to a θ value of 1.548π. Fig. 9(b) shows the measured normalized frequency response of the notch microwave photonic filter. It exhibits an extremely flat response in the passband at ultrawide frequency range of operation. The center frequency is maintained at 17 GHz. The -6-dB bandwidth is about 42 MHz, and the depth of the notch is above 42 dB. The realization of the switching function of the filter can be seen by comparing Fig. 9(a) and (b), which demonstrates switching from bandpass to notch filtering.

Next, the ability to tune the filter switching function over a wideband frequency range was experimentally demonstrated. This was done by changing the pump frequency f_p driving the IM from 11.21 to 29.21 GHz. Fig. 10 shows the measured normalized frequency response results for the bandpass filter, when the dc bias of the DDMZM was set to 0.525 V. A continuous tuning of the bandpass filter frequency from 2 to 20 GHz is demonstrated, together with shape-invariant tuning over the entire 2–20-GHz range. The filter exhibits high resolution with a -3-dB bandwidth of

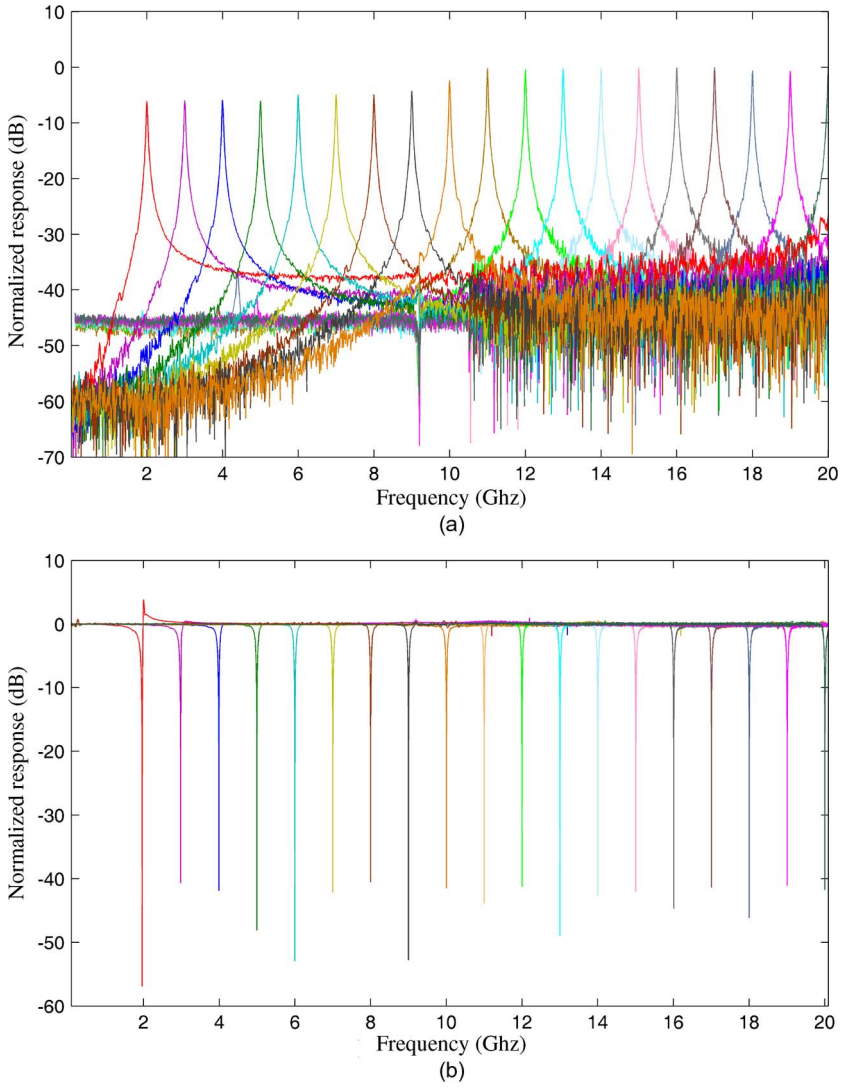

Fig. 10. Measured normalized frequency response of the switched tunable filter between (a) bandpass response; and (b) notch response.

around 32 MHz and an out-of-band rejection ratio of $>$ 30 dB over the entire tuning range. By changing the dc bias of the DDMZM to 8.591 V, which corresponds to a phase bias of 1.548π, the bandpass filter response was switched to a notch filter response. The notch filter response is shown in Fig. 10(b) at the same frequencies that correspond to the center frequencies in Fig. 10(a). The $-$6-dB bandwidth is almost constant at 41 MHz during the tuning range. It is much narrower than the bandwidth of SBS loss spectrum in the optical domain, since there is a subtraction effect during the mapping process. Moreover, the depth of the notch is $>$ 40 dB.

5. Conclusion

A new structure that realizes a switchable microwave photonic filter, which can be readily switched between a bandpass filter and a stopband notch filter, has been presented. It is based on an SBS technique in conjunction with a DDMZM that processes the sidebands of the RF-modulated signal. Switching of the filter function is simply and conveniently obtained by changing the dc bias to the DDMZM. In addition, the center frequency of the switchable filter can be tuned over a wide frequency range. A detailed analysis and simulation of the DDMZM operation in conjunction with

the SBS technique has been presented in order to obtain the required optimum bias conditions for the DDMZM in order to realize the switching action between the single-bandpass filter and the notch filter and also to select the optimum pump power for the SBS operation. Experimental results have been presented, which demonstrate the ability of this structure to switch between a high-resolution bandpass filter and a high-resolution notch filter, with Q values around 400–500, and the ability to operate over a frequency range of 2–20 GHz. To our knowledge, this is the first structure that can be switched between a high-resolution bandpass filter and a notch filter, and which can also operate over a wide frequency range.

Acknowledgment

The authors would like to thank Dr. X. Yi and Dr. T. X. H. Huang for providing the DDMZM and Dr. Q. Sun from YOFC for providing the DSF.

References

[1] R. Minasian, "Photonic signal processing of microwave signals," *IEEE Trans. Microw. Theory Tech.*, vol. 54, no. 2, pp. 832–846, Feb. 2006.
[2] J. Capmany, B. Ortega, D. Pastor, and S. Sales, "Discrete-time optical processing of microwave signals," *J. Lightw. Technol.*, vol. 23, no. 2, pp. 702–723, Feb. 2005.
[3] J. Yao, "Microwave photonics," *J. Lightw. Technol.*, vol. 27, no. 3, pp. 314–335, Feb. 2009.
[4] F. Zeng and J. Yao, "All-optical bandpass microwave filter based on an electro-optic phase modulator," *Opt. Exp.*, vol. 12, no. 16, pp. 3814–3819, Aug. 2004.
[5] J. Mora, L. Chen, and J. Capmany, "Single-bandpass microwave photonic filter with tuning and reconfiguration capabilities," *J. Lightw. Technol.*, vol. 26, no. 15, pp. 2663–2670, Aug. 2008.
[6] T. Huang, X. Yi, and R. Minasian, "Single passband microwave photonic filter using continuous-time impulse response," *Opt. Exp.*, vol. 19, no. 7, pp. 6231–6242, Mar. 2011.
[7] R. Minasian, K. Alameh, and E. Chan, "Photonics-based interference mitigation filters," *IEEE Trans. Microw. Theory Tech.*, vol. 49, no. 10, pp. 1894–1899, Oct. 2001.
[8] J. Wang and J. Yao, "A tunable photonic microwave notch filter based on all-optical mixing," *IEEE Photon. Technol. Lett.*, vol. 18, no. 2, pp. 382–384, Jan. 2006.
[9] W. Xue, S. Sales, J. Mork, and J. Capmany, "Widely tunable microwave photonic notch filter based on slow and fast light effects," *IEEE Photon. Technol. Lett.*, vol. 21, no. 3, pp. 167–169, Feb. 2009.
[10] B. Vidal, T. Mengual, and J. Marti, "Photonic microwave filter with single bandpass response based on Brillouin processing and ssb-sc," in *Proc. IEEE Int. Topical Meeting MWP*, 2009, pp. 1–4.
[11] W. Zhang and R. Minasian, "Widely tunable single-passband microwave photonic filter based on stimulated Brillouin scattering," *IEEE Photon. Technol. Lett.*, vol. 23, no. 23, pp. 1775–1777, Dec. 2011.
[12] B. Vidal, M. Piqueras, and J. Marti, "Tunable and reconfigurable photonic microwave filter based on stimulated Brillouin scattering," *Opt. Lett.*, vol. 32, no. 1, pp. 23–25, Jan. 2007.
[13] W. Zhang and R. Minasian, "Ultra-wide tunable microwave photonic notch filter based on stimulated Brillouin scattering," *IEEE Photon. Technol. Lett.*, vol. 24, no. 14, pp. 1182–1184, Jul. 2012.
[14] B. Vidal, J. Palaci, and J. Capmany, "Reconfigurable photonic microwave filter based on four-wave mixing," *IEEE Photon. J.*, vol. 4, no. 3, pp. 759–764, Jun. 2012.
[15] H. Jiang, L. Yan, J. Ye, W. Pan, B. Luo, and X. Yao, "Comb filter with independently tunable wavelength spacing and bandwidth using cascaded variable differential group delay elements," *Opt. Lett.*, vol. 36, no. 12, pp. 2305–2307, Jun. 2011.
[16] L. Yan, J. Ye, H. Jiang, W. Pan, B. Luo, A. Yi, Y. Guo, and X. Yao, "A photonic comb filter with independently and digitally tunable bandwidth and frequency spacing," *IEEE Photon. Technol. Lett.*, vol. 23, no. 13, pp. 857–859, Jul. 2011.
[17] J. Capmany, J. Cascon, D. Pastor, and B. Ortega, "Reconfigurable fiber-optic delay line filters incorporating electrooptic and electroabsorption modulators," *IEEE Photon. Technol. Lett.*, vol. 11, no. 9, pp. 1174–1176, Sep. 1999.
[18] G. Ning and P. Shum, "Switchable and tunable microwave photonic filter using a variable polarization beamsplitter in a Sagnac interferometer," *J. Opt. A, Pure Appl. Opt.*, vol. 9, no. 12, pp. 1136–1139, Dec. 2007.
[19] Y. Yu, E. Xu, J. Dong, L. Zhou, X. Li, and X. Zhang, "Switchable microwave photonic filter between high q bandpass filter and notch filter with flat passband based on phase modulation," *Opt. Exp.*, vol. 18, no. 24, pp. 25 271–25 282, Nov. 2010.
[20] A. Loayssa, D. Benito, and M. José Garde, "Applications of optical carrier Brillouin processing to microwave photonics," *Opt. Fiber Technol.*, vol. 8, no. 1, pp. 24–42, Jan. 2002.
[21] R. Boyd, *Nonlinear Optics*. New York: Academic, 2003.
[22] M. Van Deventer and A. Boot, "Polarization properties of stimulated Brillouin scattering in single-mode fibers," *J. Lightw. Technol.*, vol. 12, no. 4, pp. 585–590, Apr. 1994.